Journal of Applied Electrochemistry
https://doi.org/10.1007/s10800-022-01750-6

RESEARCH ARTICLE

Effect of 2-mercaptobenzothiazole on the corrosion inhibition of Cu–10Ni alloy in 3 wt% NaCl solution

Arman Zarebidaki[1] · **Seyed Haman Hedaiat Mofidi**[1] · **Farzaneh Iranmanesh Bahri**[1]

Received: 3 May 2022 / Accepted: 16 August 2022

Abstract

2-Mercaptobenzothiazole (MBT), a heterocyclic compound, is a remarkable corrosion inhibitor for pure Cu. Among different copper-based alloys, Cu–Ni alloys are used in a wide range of applications in industries that are exposed to the corrosive environment and making them prone to corrosion. In the current study, the effect of 2-Mercaptobenzothiazole (MBT) concentration on the corrosion inhibition of Cu–10Ni alloy in 3 wt% NaCl solution was studied using electrochemical impedance spectroscopy (EIS), potentiodynamic polarization, and weight loss methods. SEM and XPS were also used for surface characterization. Results of different methods were in good agreement and showed that MBT enhances the corrosion resistance of the alloy at concentrations of 60 and 80 ppm. At the concentration of 40 ppm, MBT deteriorates the corrosion resistance. Maximum inhibition of about 92% was achieved for the concentration of 80 ppm. MBT acts as a mixed-type inhibitor, and the N atom and exocyclic S atom of the MBT are involved in the molecule adsorption. The role of MBT in corrosion inhibition was attributed to the role of adsorbed inhibitor film, which hinders the Ni Dealloying.

Graphical abstract

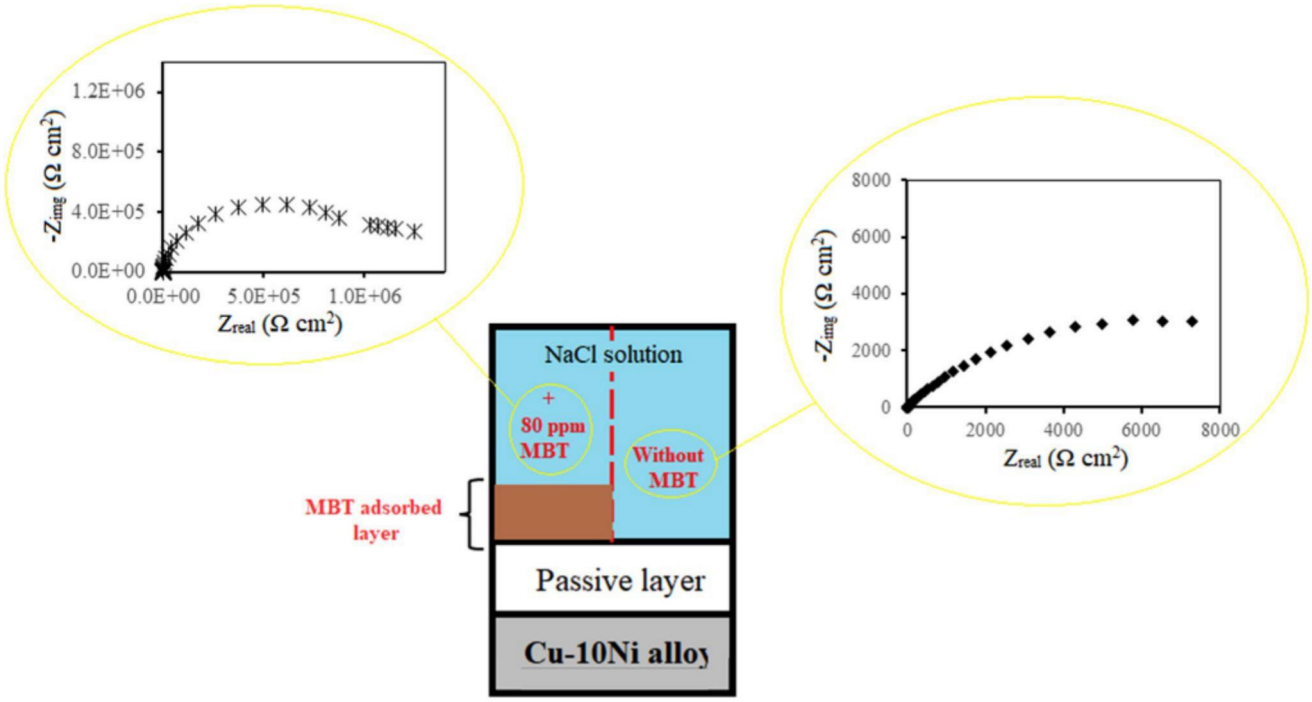

Keywords Cu–10Ni alloy · 2-Mercaptobenzothiazole · Corrosion inhibition · NaCl solution · EIS

Extended author information available on the last page of the article

Published online: 02 September 2022

1 Introduction

Biofouling resistance and good heat transfer characteristics of copper-nickel (cupronickel) alloys and their superior corrosion resistance make them the best choice for applications in marine and chemical environments. Cupronickel alloys are extensively used to fabricate ship and boat hulls, desalination plants, heat exchange equipment, seawater and hydraulic pipelines, oil rigs and platforms, fish farming cages, seawater intake screens, evaporator tubes of chilling plants, etc. [1–9]. In such aggressive applications and due to abundant use, Cu–Ni alloys, especially low Ni content alloys, are prone to corrosion in chloride-containing and polluted environments [10–12]. Corrosion inhibitors, especially organic inhibitors, are widely used to decrease the corrosion effects [12–28].

In desalination plants, the deposition of scales affects their performance and acid cleaning is performed for scale removal. Inorganic or organic acids containing inhibitors or scale removal are widely used for this purpose [20]. The effect of benzotriazole on corrosion inhibition of Cu-Ni alloys in acidic and neutral media has been investigated, and it has been shown that BTAH acts as an efficient inhibitor [11, 14, 16, 21, 26, 27].

Studies have shown that benzotriazole (BTA) can effectively decrease the corrosion rate of copper-nickel alloys in 1.5 M HCl and 60% LiBr solution and its inhibition efficiency in HCl solution is dependent on the temperature [16, 21, 24]. The maximum inhibition efficiencies of 99.8% and 86.3% were reported for BTA in 1.5 M HCl solution at 35 °C and 65 °C. It has also been reported that BTA obeys Langmuir adsorption isotherm rather than Freundlich adsorption isotherm [21, 24]. The nature of the protective film formed on the surface of Cu–10Ni alloy in deaerated 0.5 M H_2SO_4 solution containing Fe(III) ions as oxidant and benzotriazole (BTAH) as an inhibitor has been investigated by Maciel et al. They showed that a protective film is formed that is composed of cuprous benzotriazolate. BTAH adsorption obeyed Brunauer, Emmett, and Teller (BET) isotherm, which implies multi-layers adsorption. The adsorption free energy of the cuprous benzotriazolate on the surface of Cu-10Ni alloy was consistent with the value obtained for pure copper [26]. In seawater and inorganic sulfide-polluted seawater, BTAH acts as an effective mixed corrosion inhibitor even after a prolonged immersion time of 30 days. The inhibition effect of BTAH is attributed to the formation of a protective BTAH film onto the surface [19]. Studies showed that the inhibition effect of Tetraethylenepentamine (TEPA) and Napththylamine (NA) as organic inhibitors for Cu–Ni alloy in 5% HCl solution is dependent on both the temperature and solution's agitation so that the efficiency increases with decreasing the temperature and agitation level [23]. The values of activation energies obtained from the Arrhenius equation in 5% HCl solution containing NA and phenylenediamine (PDA) showed that activation energy corresponding to the former inhibitor is dependent on its concentration. It has also been shown that the variations of activation energy in the presence and absence of an inhibitor indicate the inhibitive efficiency so that the higher increment implies higher inhibition effect [12, 21]. For Cu–Ni alloys in 5% HCl solution, the activation energy of NA adsorption is dependent on its concentration so that the changes of the activation energy in the presence and absence of an inhibitor can indicate the inhibitive efficiency so that higher activation energy implies a higher inhibition effect [12, 21]. Shiffbase inhibitors were used for corrosion inhibition of copper alloys and it was shown that the presence of thiol group (–SH) or amine group ($–NH_2$) leads to the formation of stable complexes and the high inhibition effect [29]. Propargyl alcohol can act as an organic inhibitor for corrosion inhibition of copper-nickel alloys in 0.50 M sulphuric acid and its role depends on the adsorption potential and alcohol concentration [14].

Heterocyclic organic compounds such as azole derivatives are widely used for corrosion inhibition of copper and copper alloys [12, 30–34]. Azoles are organic compounds containing nitrogen atoms with free electron pairs, and there is the possibility of introducing other heteroatoms and groups in molecules of these compounds. 2-Mercaptobenzothiazole (MBT; $C_6H_4(NH)SC{=}S$) as an azole derivative is a planar organosulfur compound with a C=S double bond. MBT involves N and S atoms in the ring and an S atom in the thiocarbonyl group available for coordination. In an alkaline medium, the S atom of the thiocarbonyl group is ionized and reacts with Cu to form a thick polymeric film. It has been reported that azole derivatives are the potential inhibitor with high inhibiting efficiency for pure copper [35]. Sutter et al. have shown that in corrosion inhibition of copper by aromatic heterocyclic compounds, the nature of the binding between Cu(I) and the organic molecule and the properties of the copper oxide has to be considered to understand the inhibiting mechanism [36]. 2-mercaptobenzimidazole (MBI) acts as an excellent mixed-type inhibitor that hinders the anodic and cathodic reactions of Cu–30Ni alloy in 3% NaCl solution polluted with ammonia [37].

Quantum chemical calculations and electrochemical measurements have shown that triazole-based inhibitors include 1,2,4-triazole (TA), 3-amino- 1,2,4-triazole (ATA), and 3-amino-5-mercapto-1,2,4-triazole (AMT) exhibit good corrosion inhibition efficiency for Cu-10Ni alloy in 3.5 wt% NaCl solution. The inhibition efficiency of these mixed-type inhibitors increases with increasing their concentration up to 1 mM. It has been suggested that the triazole ring and the heteroatoms act as active centers for adsorption of the

compound through donating electrons to the unfilled hybrid orbital of copper atoms which would lead to the formation of an inhibitor film that contributes to high inhibition efficiency [22]. The effects of sulfide (HS^-) ions on the corrosion inhibition of Benzotriazole (BTAH) for Cu–10Ni alloy in 3.4% NaCl solution have been investigated by Allam et al. Their study showed that due to the competitive adsorption of sulfide ions and BTAH onto the alloy surface, the presence of the ions decreases the inhibiting efficiency of BTAH [38]. The structure of the passive film formed on Cu-10Ni alloy in sodium acetate solution (pH 5.8) consisted of an outer CuO/$Cu(OH)_2$ layer overlaying a barrier Cu_2O layer. It has been revealed that in this condition, BTAH acts as an effective inhibitor even at a very low concentration [39].

Inhibition effects of Sodium diethyldithiocarbamate ($NaEt_2dtc$) as an organosulfur compound for corrosion inhibition of Cu–10Ni alloy exposed to quiescent natural seawater and jet impingement seawater with different fluid velocities have been investigated by Martinez et al. They showed that the inhibition mechanism includes the formation of a surface chelate compound between the dissolving metal ion and the (Et_2dtc)) ligand, as well as the formation of a 3-D ternary surface insoluble complex. It is also revealed that $NaEt_2dtc$ yields excellent inhibiting efficiency (> 90%) in hydrodynamic conditions [28].

Amino acid compounds such as glycine, alanine, and leucine as aliphatic amino acids, cysteine as sulfur-containing amino acids, lysine and histidine as basic amino acids, and glutamic acid as acidic amino acid showed remarkable corrosion inhibition effect Cu–Ni alloys in aqueous chloride solution. These compounds shift the OCP in the negative direction and resemble a cathodic inhibitor.

Between these compounds, cysteine with two adsorption centers, including a heterocyclic ring and/or π–electron, induces and enhances the adsorption of the inhibitor onto the metallic surface [27, 40]. The effects of some amino acids, including glycine, alanine, leucine, cysteine, glutamic acid, lysine, and histidine, on the corrosion inhibition of Cu–5Ni and Cu–65Ni alloys in acidic sulfate solutions have been studied by Waheed et al. Their investigation revealed that the corrosion inhibition of these compounds depends on the Ni content of the alloy as well as the structure of the amino acid. It was shown that long-chain non-branched amino acids are more effective in corrosion inhibition, and the adsorption of amino acids is enhanced in the presence of iodide ions [41].

MBT, as a heterocyclic compound, is known as a remarkable corrosion inhibitor for pure Cu. The presence of S, N, and O heteroatoms in the ring of MBT leads to a strong coordination bond and its superior inhibition efficiency for Cu [35, 42–50]. There is no report that investigated the effect of MBT concentration on the corrosion inhibition of Cu–Ni alloys in 3 wt% NaCl solution through weight loss, potentiodynamic polarization, and EIS methods. The nature of the film formed on the specimen's surface has also been investigated by XPS, SEM, and EDAX.

2 Materials and methods

Annealed sheet of Cu-10Ni (Cu: 89.0 wt%, Ni:10.8 wt%, Fe:0.04 wt%) alloy with the thickness of 3 mm was used for preparing the specimen with proper dimensions. The electrolytes used for tests were 3 wt% NaCl solution (blank solution) and 3wt% NaCl solution containing 40, 60, and 80 ppm of 2-Mercaptobenzothiazole (MBT). The test specimens were carefully polished using SiC abrasive paper with the grit size of 100–1500, degreased with acetone, rinsed with distilled water, and dried with air blow. Each prepared specimen was instantly immersed in 250 ml of the relevant solution.

For the weight loss test, specimens with the dimension of 1 cm × 2 cm × 3 mm were cut from the annealed sheet, abraded with SiC abrasive papers (grit size #800 to #1500), and washed with distilled water. The specimens were degreased with acetone and rinsed with distilled water, and finally dried with air blow. The prepared specimens were weighted in the precision of 4 decimal places and immersed in 400 ml of the aforementioned solutions for 30 days and then removed from the solution. The corrosion products were removed by immersing in deaerated 1 M HCl under ultrasonic agitation. Weight loss measurements were performed in triplicate for each condition. Corrosion rate (v) and inhibition efficiency (IE%) were calculated as follows:

$$v = \frac{w_0 - w}{\mathrm{S.t}} \tag{1}$$

$$\mathrm{IE\%} = \frac{v_0 - v}{v_0} \tag{2}$$

where w_0 and w are the weights before and after immersion, and S and t represent the total surface area (cm^2) exposed to the solution and total time (day) of exposure. In Eq. 2, v_0 and v represents the corrosion rate ($mgcm^{-2}day^{-1}$) at the presence and absence of inhibitor, respectively.

X-ray Photoelectron Spectroscopy (XPS) study was performed on the specimens (10 cm × 20 cm × 3 mm) immersed in 3 wt% NaCl solution containing 80 ppm MBT for 48 h using PHI 5700 spectrometer with Al K_α of X-ray radiation source (1486.6 eV). The energy of the emitted photoelectrons was measured with an electron analyzer operating at the pass energies of 29.3 eV and 58.7 eV for high-resolution spectra and 187.8 eV for survey spectra. The pressure of the spectrometer was 2×10^{-10} mbar. The spectrometry was performed at 90° against the sample surface. The peaks were

calibrated using adventitious carbon peak C 1*s* at the binding energy of 248.8 eV. The extracted data were studied using OriginPro 2019b (version 9.6.5.169) for Shirley's background subtraction of all the high-resolution (HR) spectra. The estimated accuracy in binding energy measurement was 0.2 eV. No sputtering process was used before spectrometry. SEM equipped with energy-dispersive X-ray spectroscopy (EDAX) was used to study the surface of the specimens.

For conducting the electrochemical tests, specimens (10 mm × 10 mm × 3 mm) were electrically connected and embedded in two-body epoxy resin so that the 1 cm^2 area of each specimen could be exposed to the electrolyte. The EIS tests were conducted after 48 h of immersion in 3 wt% NaCl solution to ensure reaching a steady state in the absence and presence of MBT (40, 60, and 80 ppm). EIS tests were performed at the open circuit potential (OCP), using 5 mV amplitude sinusoidal voltage in the frequency range of 10 kHz–0.01 Hz. Potentiodynamic polarization tests were also conducted after 48 h of immersion for all the specimens at the potential range of − 250 mV to + 450 mV vs. OCP at the scan rate of 10 mV s^{-1}. TOFEL extrapolation method was used to determine the corrosion-related information from the polarization tests using NOVA 2.1.2 software. The tests were conducted in a standard three-electrode cell using an Autolab/PGSTAT 302 N instrument equipped with a frequency response analyzer (FRA) module. A Platinum plate and an Ag/AgCl electrode were used as the counter and the reference electrodes, respectively. The equivalent circuit simulation program (ZView2) was used for data analysis, synthesis of the equivalent electrical circuit (EEC), and fitting of the experimental data.

3 Results and discussion

3.1 Weight loss results

The corrosion rate of Cu–10Ni alloy in 3% wt NaCl solution as a function of MBT concentration are summarized in Table 1. It is seen that the corrosion rate of Cu–10Ni alloy increases at the presence of 40 ppm MBT and then decreases with increasing the MBT concentration up to 80 ppm. This behavior might be attributed to the desorption of the inhibitor molecules or the lack of the presence of a continuous adsorbed inhibitor film in low inhibitor concentration.

It can be seen that there is a critical concentration above which the inhibition effect is revealed. The maximum inhibition efficiency of about 90% is achieved for the specimen immersed in the solution containing 80 ppm MBT.

Table 1 Corrosion rate and inhibition efficiency of MBT obtained for Cu–10Ni alloy in 3 wt% NaCl solution in the absence (blank) and presence of MBT

MBT concentration	Corrosion rate (g m^{-2} day^{-1})	% IE
Blank	0.6374 ± 0.0228	–
40 ppm	0.65731 ± 0.0264	− 4 ± 0.5
60 ppm	0.30299 ± 0.0157	57 ± 2
80 ppm	0.06551 ± 0.0004	90 ± 0.01

3.2 XPS analysis

Figure 1 shows the XPS spectrum of the specimen immersed for 48 h in 3 wt% NaCl solution containing 80 ppm MBT. Peaks represent Na, Cu, Ni, O, N, C, S, and Cl species. Na 1*s* peak at binding energy (E_B) of 1073 eV, X-ray-induced auger Na KLL at E_B of 498.8 eV, and Cl 2p peak at E_B of 201.2 eV (peaks determined according to NIST XPS database [51]) indicates the presence of NaCl residue on the surface even after thorough rinsing of the specimen with distilled water. Cl 2*p* peak can also indicate the presence of CuCl and $CuCl_2$ as corrosion products. Cu 3*p*, Cu 2*p*, and Cu LMM peaks can be originated from Cu, Cu oxides, $CuCl_2$, $Cu(OH)_2$, and Cu-complexes with MBT inhibitors. According to the NIST XPS database, the positions of Cu 2p3/2 for the $Cu(OH)_2$, Cu_2O, and CuO are at E_B of 932.7–935.1 eV, 932.0–932.8 eV, and 932.7–934.4 eV, respectively. Moreover, Cu 2*p*3/2 position for CuCl and $CuCl_2$ is reported to be at E_B of 932.20–932.60 eV and 934.0–935.6 eV, respectively. The presence of CuCl and $CuCl_2$ is probable due to the peaks at the lines (1 and 2) shown in Fig. 2. The shoulder on the high E_B side (line 2) in Fig. 2 probably corresponds to $CuCl_2/Cu(OH)_2$ compounds. The presence of Cu oxides will be discussed further in O 1*s* peak analysis.

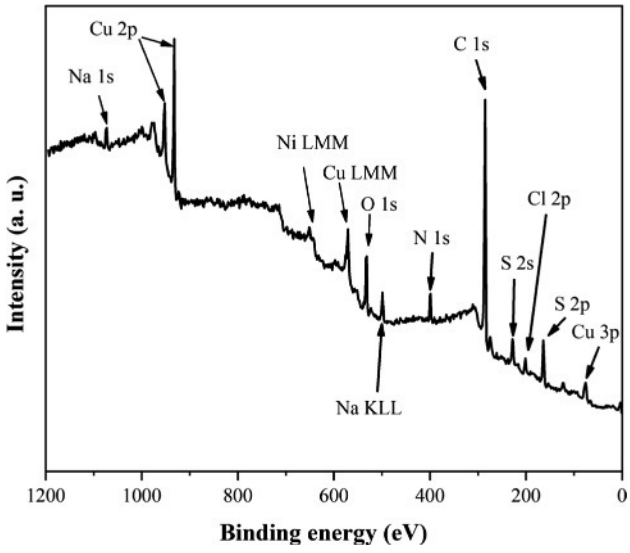

Fig. 1 XPS survey spectrum of Cu–10Ni specimen immersed in 3 wt% NaCl solution containing 80 ppm MBT after 48 h of immersion

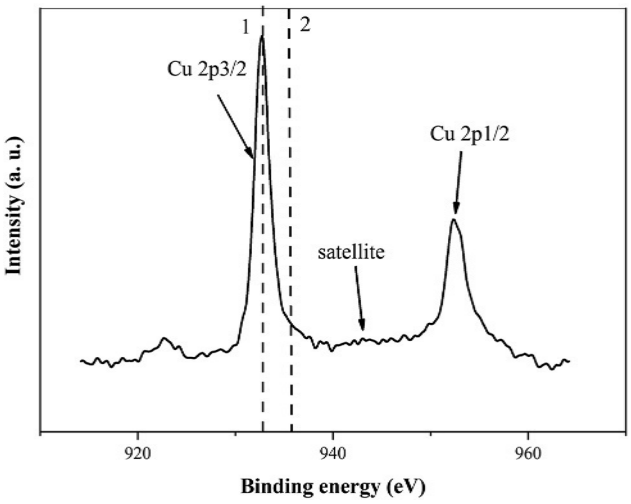

Fig. 2 XPS Cu 2*p* spectrum of Cu–10Ni specimen immersed in 3 wt% NaCl solution containing 80 ppm MBT after 48 h of immersion

The shake-up satellites correspond to the existence of Cu(II) species, but the amount is probably low compared to Cu(I) species, which mainly formed the Cu 2*p* peaks. The N 1*s* peak (Fig. 3) corresponds to the nitrogen in MBT inhibitor ($C_6H_4(NH)SC{=}S$). The small shoulder on the high E_B side can be related to the second environment for nitrogen. It is probably due to the attachment of the inhibitor to the surface through the N atom.

Two different environments can be detected from the C 1*s* peak shown in Fig. 4. The peak at E_B of 285 eV could imply the non-oxidized carbon from the surface contamination comprised C–C groups. These are carbon-containing molecules that are physisorbed via van der Waals interaction to the sample's surface before XPS. It could also imply the C–C bonds in the MBT molecules. The peak with higher E_B could correspond to the oxidized carbonaceous spices from the atmosphere usually adsorbed on the metal surfaces [52]. O 1*s* peak is shown in Fig. 5 at E_B of ≈ 834.4 eV. The O 1*s* peaks of CuO and Cu_2O are at E_B of 529.5–530.0 and 530.2–531.1 eV. Therefore, it is evident that they should be excluded from the compounds on the surface of the sample. The position of O 1*s* for $Cu(OH)_2$ is 530.9–531.5 eV. According to the XPS NIST database, this peak mainly applies to $Cu(OH)_2$ and organic C–O groups, as aforementioned. There seem to be three distinct environments on the surface of the sample (Fig. 6). All three environments could be derived from the sulfur of the MBT molecules. According to previous research on MBT attachment on the metal surface [53], both N and S can link to the surface. Therefore, free inhibitor on the topmost layer attached inhibitor to the surface through S and N and MBT complexes is the most probable source of the distinct peaks of sulfur in S 2*p* spectrometry. The interaction between MBT and the surface of the metal is complex since the different forms of MBT, including thiol, thione, and anionic forms, can interact with the surface through different active sites, including S, N, and NH. The interaction between MBT and surface depends on the surface state. In an environment with pH > 4 due to the presence of copper oxide, a monolayer of MBT film forms on the surface. Two sulfur atoms of MBT can form a chemical bond on Cu (220) surface, while on Cu(200) and Cu(111) surfaces, electrostatic interactions lead to the physical bonding of the MBT [54]. Terminal S atom can

Fig. 3 XPS N 1*s* spectrum of Cu–10Ni specimen immersed in 3 wt% NaCl solution containing 80 ppm MBT after 48 h of immersion

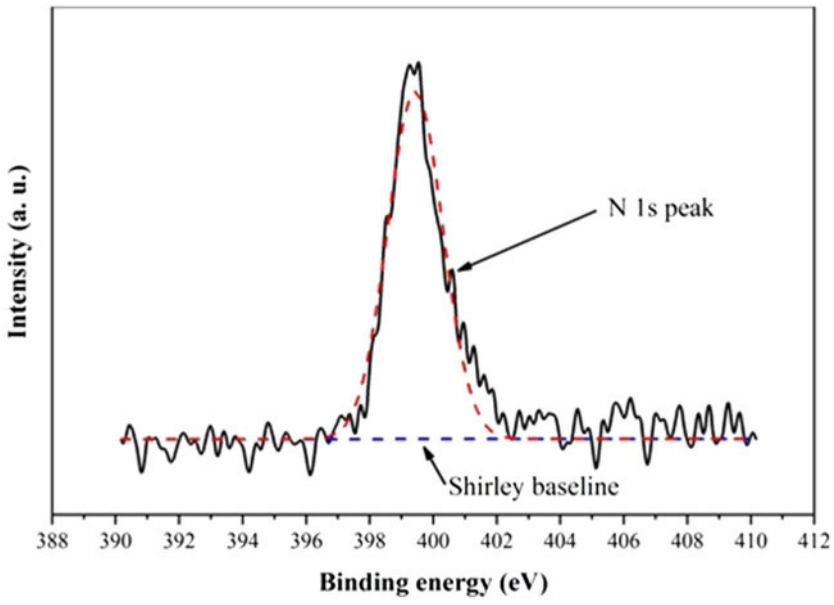

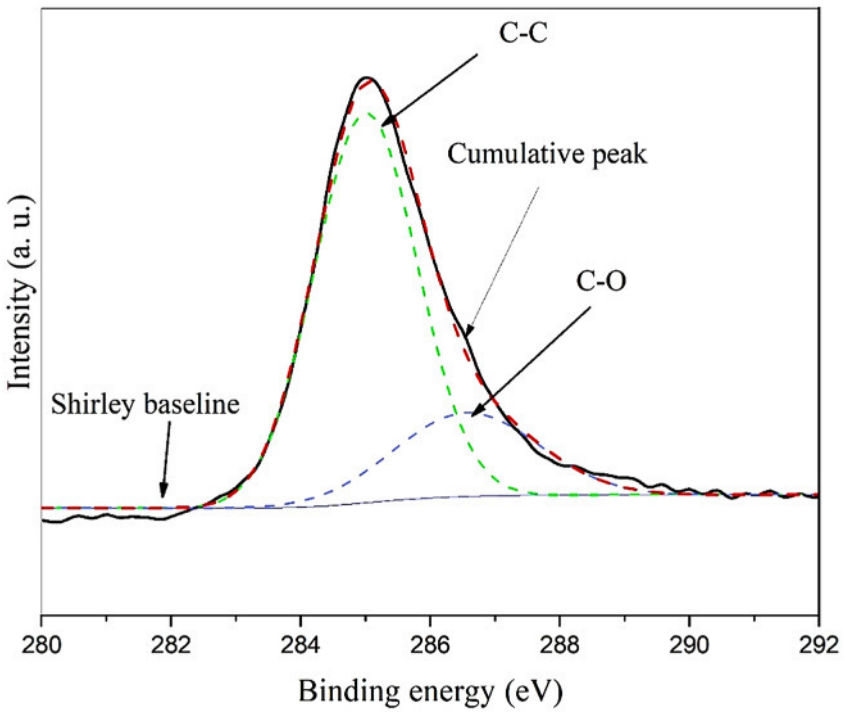

Fig. 4 XPS C 1*s* spectrum of Cu-10Ni specimen immersed in 3 wt% NaCl solution containing 80 ppm MBT after 48 h of immersion

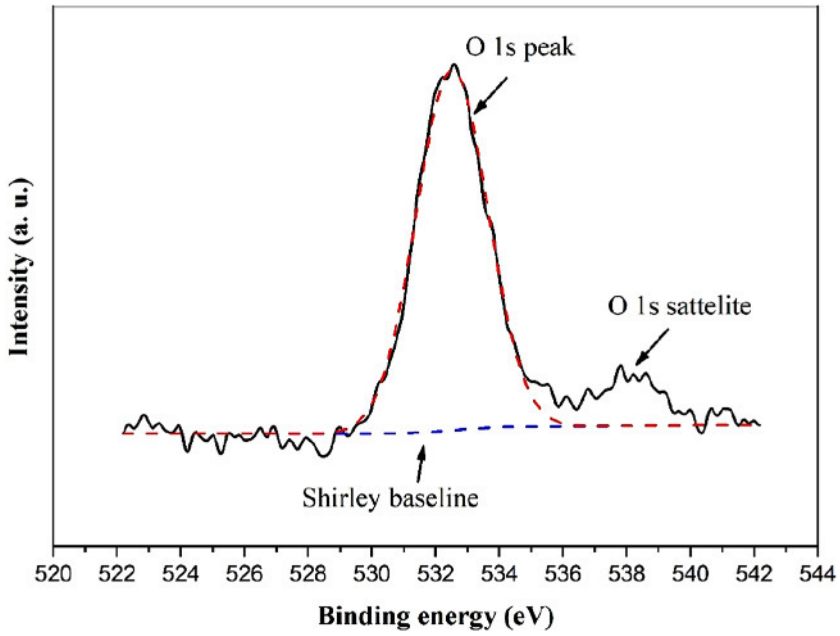

Fig. 5 XPS O 1*s* spectrum of Cu-10Ni specimen immersed in 3 wt% NaCl solution containing 80 ppm MBT after 48 h of immersion

be strongly adsorbed in a perpendicular orientation at high coverage on the Cu(111) surfaces [55]. So it seems that the S atoms have a more influential role in the corrosion inhibition yielded by MBT.

3.3 Potentiodynamic polarization test results

Potentiodynamic polarization curves obtained for the specimens immersed in 3 wt% NaCl solution containing different concentrations of MBT are shown in Fig. 7. The corrosion parameters are also presented in Table 2. The inhibition efficiency (%IE) was also calculated by Eq. 3 using the results of the polarization test.

$$\mathrm{IE}\% = \frac{i_{corr,0} - i_{corr}}{i_{corr,0}} \times 100 \tag{3}$$

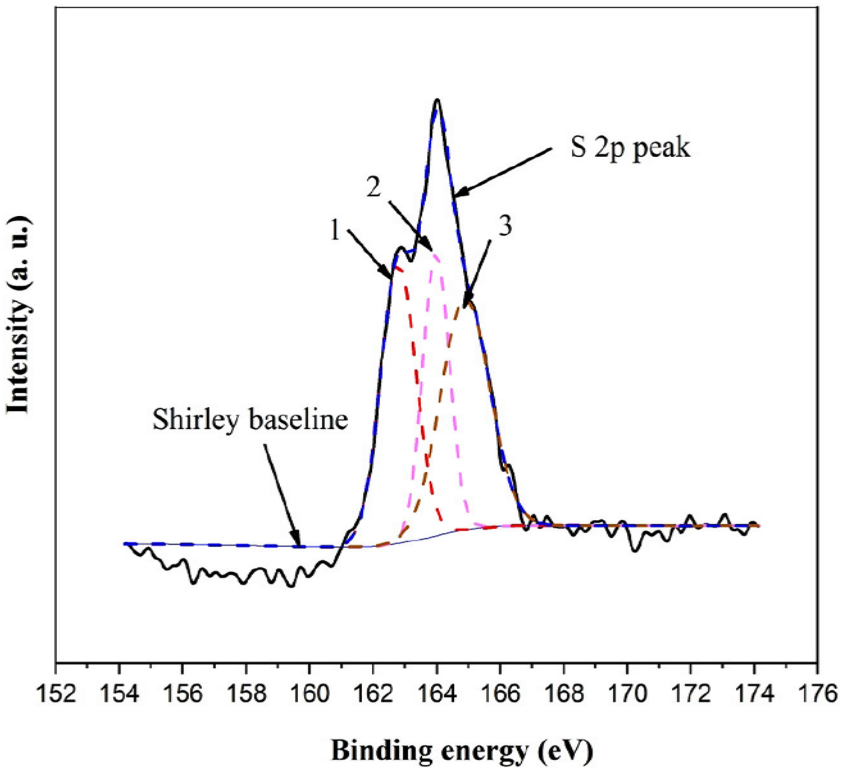

Fig. 6 XPS S 2*p* spectrum of Cu-10Ni specimen immersed in 3 wt% NaCl solution containing 80 ppm MBT after 48 h of immersion

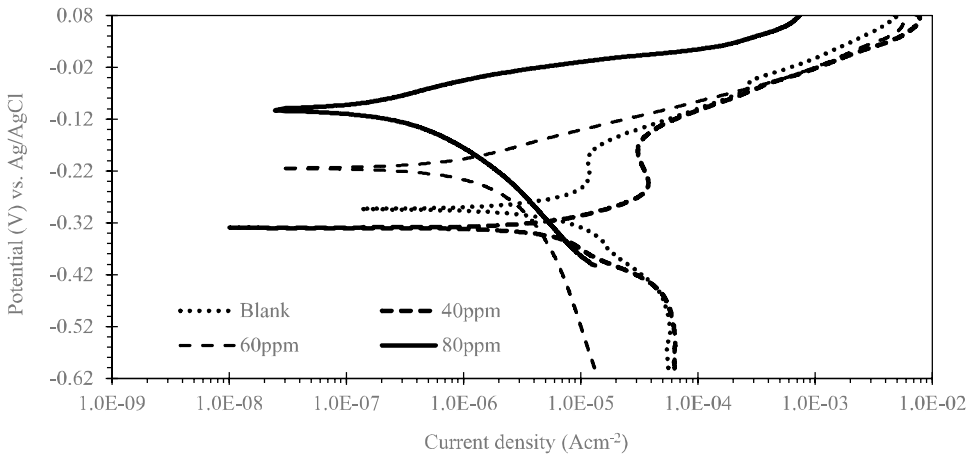

Fig. 7 Potentiodynamic polarization curves obtained for Cu–10Ni alloy in 3 wt% NaCl containing different concentrations of MBT measured after 48 h of immersion

Table 2 The corrosion parameters curves obtained for Cu–10Ni alloy in 3 wt% NaCl containing different concentrations of MBT measured after 48 h of immersion obtained from polarization curves

C (ppm)	E_{corr} (mV)	i_{corr} (μA cm^{-2})	IE%
Blank	− 280	4.5	–
40	− 330	6	− 33
60	− 180	3	33
80	− 80	0.28	93

where i_{corr} and $i_{corr,0}$ represent the corrosion current density of the specimens in the presence and absence of the inhibitor, respectively. It is seen that the corrosion current density of the specimen immersed in the solution containing 40 ppm MBT is higher than the density obtained for the blank solution, which is consistent with the weight loss test result. At higher concentrations, the corrosion current density decreases compared to the blank solution.

The highest inhibition efficiency of 93% is available for the solution containing 80 ppm MBT, which is equal to the value obtained from the weight loss test. Comparing the E_{corr} values of the specimens shows that the corrosion potential shifts toward the anodic direction when the MBT concentration is higher than 40 ppm. For the specimens immersed in the electrolytes containing 60 and 80 ppm MBT, the current density of both cathodic and anodic branches decreases at the whole applied potential. This behavior confirms that MBT acts as a mixed inhibitor.

In chloride-containing solution, the cathodic reactions of Cu–Ni alloy could be the reduction of water and the reduction of oxygen as the following equations [56]:

$$O_2 + 2H_2O + 4e^- = 4OH^- \quad (4)$$

$$2H_2O + 2e^- = H_2 + 2OH^- \quad (5)$$

In neutral NaCl solution, the corrosion of Cu–Ni alloy proceeds through the dissolution of $CuCl_{ads}^-$ adsorbed layer, formed on the surface, especially under cathodic polarization, and leads to the formation of soluble $CuCl_2^-$. With increasing the $CuCl_2^-$ concentration, Cu_2O passive layer forms from its hydrolysis, and the corrosion rate decreases [57]. Compared to the passive film of pure Cu, the passive film forms on the surface of Cu-Ni alloys include Ni ions (as shown in XPS analysis). The incorporation of Ni ion into the passive film (Cu_2O) reduces the number of cation vacancies and p-type holes that normally exist in the oxide [57, 58]. In the polarization curves of the specimens immersed in the blank solution and the solution containing 40 ppm MBT, a passive region in a short potential interval is identified, which is attributed to the formation of $CuCl_{ads}^-$ adsorbed layer and the formation of Cu_2O passive layer due to its hydrolysis [1, 18, 41, 46–48]. The Ni content of the Cu_2O film is firmly time-dependent. The initially formed Cu_2O film is quite rich in Ni ions, and after reaching the equilibrium, which is obtained very fast, Ni ions are preferentially leached out or a new Cu_2O film with lower Ni content forms [59]. So the presence of a short interval of the passive region could be attributed to the rapid preferential leach out of Ni.

For the specimens immersed in the solutions containing more than 40 ppm MBT, the anodic behavior is slightly different, which implies that the anodic process is affected by MBT. In the presence of 60 ppm and 80 ppm of MBT due to the formation of the adsorbed inhibitor film on the surface, the step of $CuCl_{ads}^-$ adsorption might be ceased. The rate of anodic dissolution of copper in NaCl solution is dependent on the diffusion rate of $CuCl_2^-$ toward the solution and the presence of insoluble corrosion products on the surface can not prevent the reduction of oxygen [60, 61]. The decreasing of the anodic and cathodic current densities in the solutions containing 60 ppm and 80 ppm MBT is the result of the adsorption of MBT molecules onto the surface of the specimen, which hinders the anodic and cathodic reactions as well as decreasing the diffusion rate of corrosion products toward the solution or reactive species toward the specimen surface. The inhibition effect of MBT is attributed to the presence of three hetero atoms in the MBT molecular structure. These heteroatoms involve N and S atoms in the thiocarbonyl group and another S atom in the thiazole ring. The copper atom has a vacant d orbital and accepts electrons from the heteroatoms, which results in a strong bond [53].

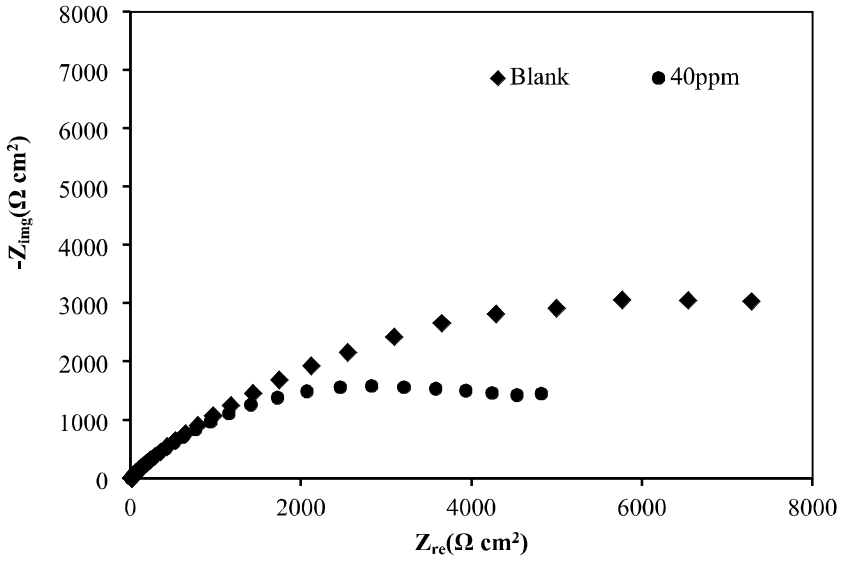

Fig. 8 Nyquist plots of Cu–10Ni alloy specimen after 48 h of immersion in blank solution and solution containing 40 ppm MBT

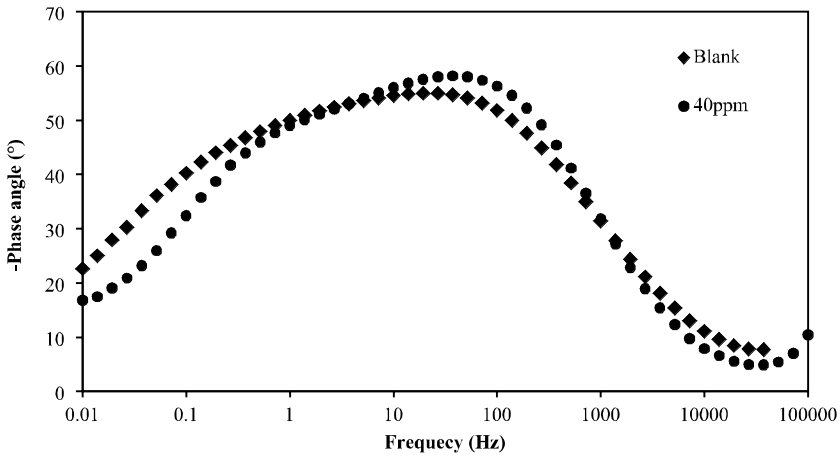

Fig. 9 Bode-phase plots of Cu–10Ni alloy specimen after 48 h of immersion in blank solution and solution containing 40 ppm MBT

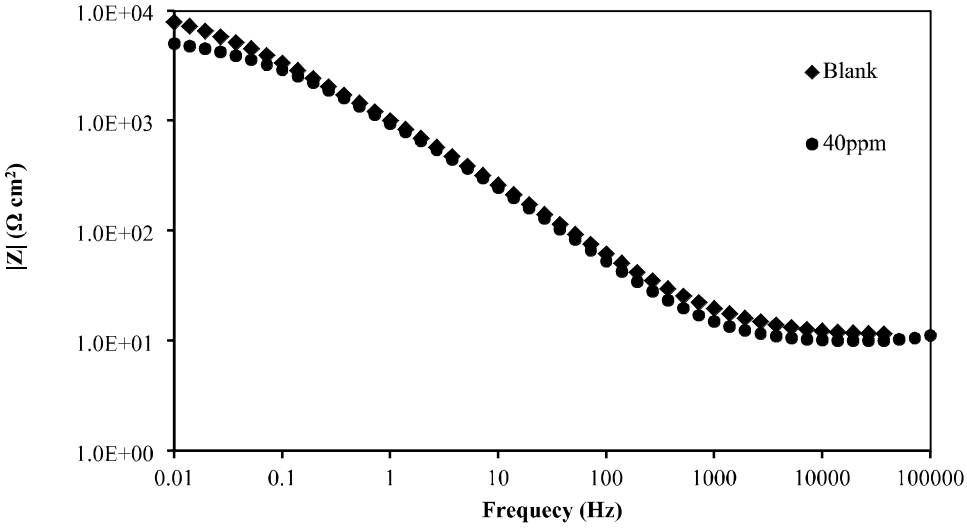

Fig. 10 Bode-modulus plots of Cu–10Ni alloy specimen after 48 h of immersion in blank solution and solution containing 40 ppm MBT

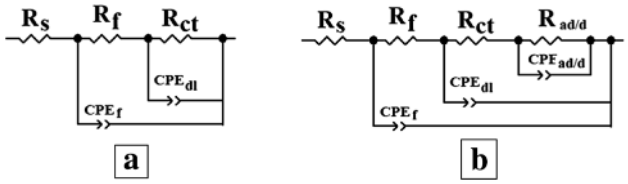

Fig. 11 EEC was used to fit the impedance results obtained for Cu–10Ni alloy specimen after 48 h of immersion in **a** blank solution and **b** solution containing 40 ppm MBT

3.4 EIS result

Nyquist, Bode-phase, and Bode-modulus plots obtained for Cu-10Ni after 48 h of immersion in blank and 40 ppm MBT-containing solutions are shown in Figs. 8, 9, and 10. The best EECs fit the corresponding EIS results are shown in Fig. 11a and b.

In the high-frequency region of the Bode diagrams (Figs. 9 and 10), the impedance reaches approximately a constant value independent of the frequency, and the phase angle tends towards 0°, which resembles the uncompensated or solution resistance (R_s). In the middle-frequency region, impedance and the frequency show a linear relationship, and the phase angle tends to -60°. In the low-frequency region, impedance tends to become independent of the frequency, but constant amplitude is not reached, and the phase does not approach 0°, which can be attributed to the diffusion of the ionic species through the passive film formed onto the surface.

The proposed EEC model to fit the data obtained for the specimen immersed in blank solution (Fig. 11a), involves two time-constants in series with the solution resistance (R_s). The first time-constant (R_fCPE_f) represents the properties of the passive film and the second time-constant in the low-frequency region represents the charge-transfer resistance

Table 3 Parameters obtained from fitting the EIS data obtained for Cu–10Ni alloy specimen after 48 h of immersion in blank solution and solution containing 40 ppm MBT to the proposed EEC

Solution	R_s (Ω)	R_{ct} (kΩ cm^2)	CPE_{dl}		C_{dl} (μF cm^{-2})	CPE_f		C_f (μF cm^{-2})	R_f (kΩ cm^2)	$CPE_{ad/d}$		$C_{ad/d}$ (μF cm^{-2})	$R_{ad/d}$ (kΩ cm^2)	R_p (kΩ cm^2)	χ^2 ($\times 10^{-4}$)
			Q ($\times 10^{-5}$)	n		Q ($\times 10^{-5}$)	n			Q ($\times 10^{-5}$)	n				
Blank	9.98	9.485	19.109	0.55		22.40	0.67		2.267	–	–	–	–	11.76	2.7
40 ppm/48 h	9.57	4.480	21.338	0.61	0.04578	14.69	0.76	1.0211	0.7256	1152.7	0.7	542.6	3.14	8.35	0.79

and the constant phase element related to the double-layer capacitor at the metal surface.

The EEC model used to fit the data obtained for the specimen immersed in 3 wt% NaCl solution containing 40 ppm MBT (Fig. 11b) corresponds to an electrode coated by a porous layer, including diffusion. Similar models have been used to explain Cu corrosion behavior in different solutions [62]. The value of EEC parameters is presented in Table 3. It should be noticed that various other EEC models were used to fit the experimental data, but the goodness of the fitting procedure, which was judged by the χ^2 value, was worse than the proposed model, and the proposed ECC gave a reasonable value for the parameters. In Fig. 11b, R_s, R_{ct}, and R_f represent solution resistance, charge-transfer resistance, and adsorbed inhibitor film resistance, respectively. CPE refers to the constant phase element, and subscripts dl, f, and ad/d represent the double-layer, adsorbed inhibitor film, and adsorption/desorption or diffusion processes.

The EEC model proposed to fit the EIS results of the specimen immersed in the electrolyte containing 40 ppm MBT involves three time-constants in series with the solution resistance (R_s). The first time-constant in the high-frequency region (R_fCPE_f) represents the properties of the passive film, and the corresponding R_f and CPE_f represent film resistance and the constant phase element related to the film capacitor. The impedance of CPE defines as follows:

$$Z(\mathrm{CPE}) = (Q(\mathrm{j}\omega)^n)^{-1} \tag{6}$$

where Q is the frequency-independent real constant (equal to the numerical value of the admittance (1/|Z|) at $\omega = 1$ rad/s), j is the imaginary number ($j^2 = -1$), ω is the angular frequency ($\omega = 2\pi f$), and n is the CPE power. The phase angle of the CPE, α, is calculated as $n = \alpha/(\pi/2)$. For an ideal capacitor, $n = 1$, and when $n = 0$, CPE resembles a pure resistor. Surface heterogeneity and roughness, inhomogeneous reaction rates on the surface, varying thickness or composition of the surface, non-uniform current distribution, and distribution of the time-constants can lead to $0 < n < 1$ [56, 63–66]. True capacitance (C) of the time-constant is calculated from CPE parameters and its parallel resistor as follows:

$$C = \left((RQ)^{1/n}\right)/R, \tag{7}$$

where R and Q are in Ω and $\mu\Omega^{-1}$ cm^{-2} s^n, respectively [67].

The second time-constant in the high-frequency region ($R_{ct}CPE_{dl}$) represents the charge-transfer process, and the corresponding R_{ct} and CPE_{dl} represent charge-transfer resistance and the constant phase element related to the double-layer capacitor. The third relaxation process, $CPE_{ad/d} - R_{ad/d}$, is related to the adsorption/desorption process of the MBT

on the alloy's surface or the diffusion process. It has been reported that a capacitance value of around 100–1000-times higher than C_{dl} corresponds to the adsorption capacitance [68, 69]. Cu and Ni ions and their complexes formed during the corrosion process are the most likely ions that diffuse through the adsorbed inhibitor film. The time-constants representing the adsorption/desorption and diffusion processes are too close and overlapped, so it is impossible to detect them separately.

The polarization resistance (R_p) value is calculated as the sum of all R-fitted parameters ($R_p = R_{ct} + R_f + R_{ad/d}$). For the specimen immersed in the solution containing 40 ppm MBT, the adsorbed inhibitor film cannot provide an effective protective ability and cannot hinder the Ni dealloying.

Comparing the R_p values of the specimens immersed in the blank solution ($R_p = 11.76$ KΩ cm^2) and the solution containing 40 ppm MBT ($R_p = 8.35$ KΩ cm^2), reveals that the addition of inhibitor has a deteriorating effect on the corrosion resistance ($R_{p,blank} > R_{p,inhibited}$) which is consistent with the weight loss and polarization tests results.

The SEM micrographs of the Cu-10Ni alloy specimens before and after 48 h of immersion in the blank solution and the solutions containing 40 and 80 ppm MBT are shown in Fig. 12. It is seen that the specimen immersed in the solution containing 80 ppm MBT has undergone a mild corrosion attack compared to the specimen immersed in the solution containing 40 ppm MBT so that the grooves of the preparing treatment are sharply visible for the former. The higher corrosion rate of the specimen immersed in the solution containing 40 ppm MBT might be related to the adsorption/desorption of the inhibitor or a more localized corrosion attack (arrows in Fig. 12c) due to the lack of the formation of a continuous protective layer of the inhibitor. Severe and more localized attacks are evident in Fig. 12c. The EDAX analysis of the surface shows that the Ni content is affected by the immersion condition. Before immersion, the nickel content is about 10 wt%, while for the specimen immersed in the blank solution and the solution containing 40 ppm MBT, the Ni content obtained around 5 wt% and 7 wt%, respectively, which confirms Ni Dealloying. For the specimen immersed in the solution containing 60 and 80 ppm

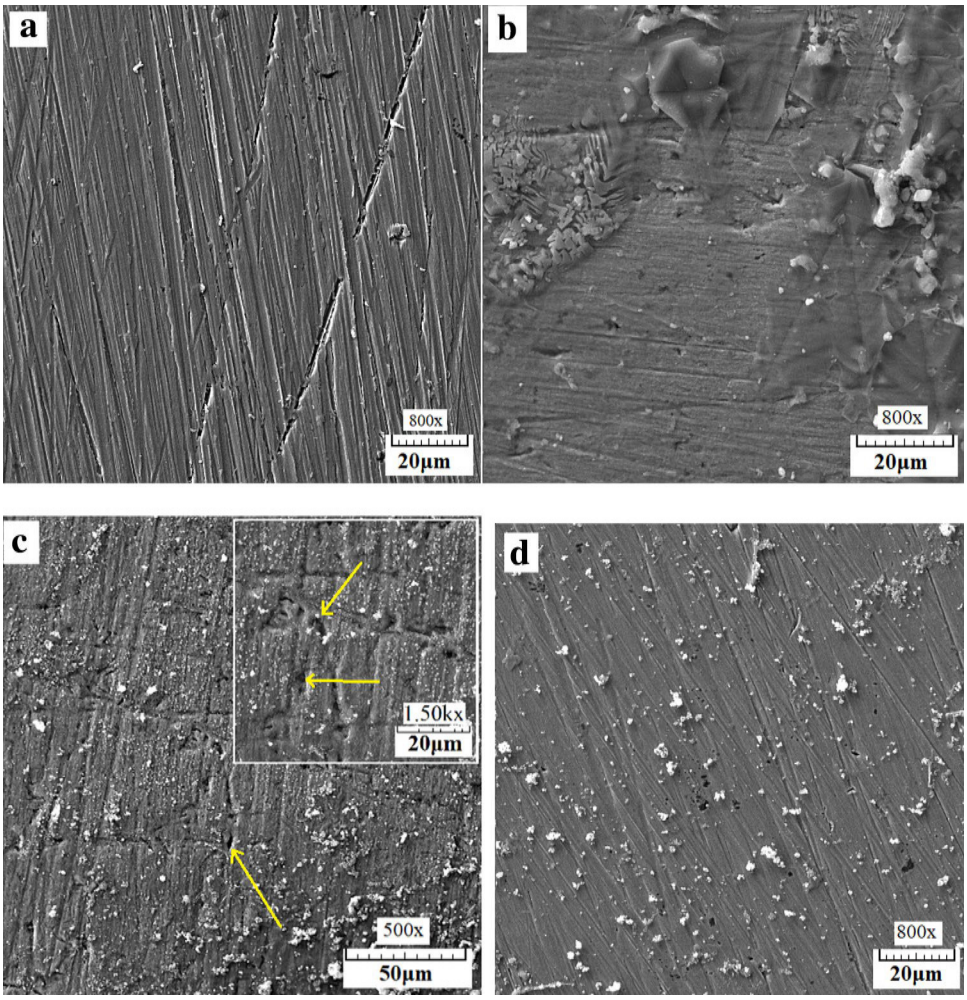

Fig. 12 SEM micrographs of Cu–10Ni alloy specimens before immersion (**a**) and after 48 h of immersion in 3 wt% NaCl solution (**b**) and the solution containing 40 ppm MBT (**c**) and 80 ppm MBT (**d**)

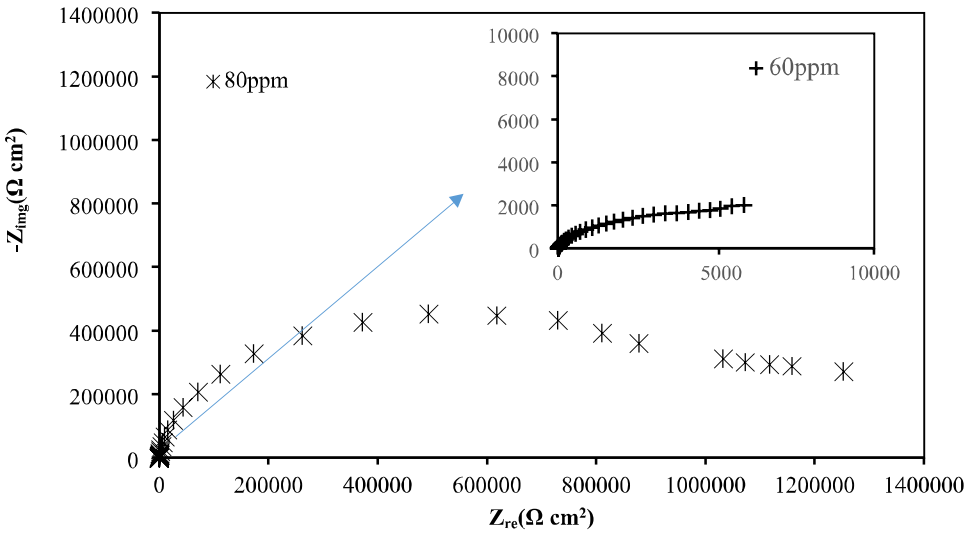

Fig. 13 Nyquist plots of Cu–10Ni alloy specimen after 48 h of immersion in blank solution and solution containing 40 ppm MBT

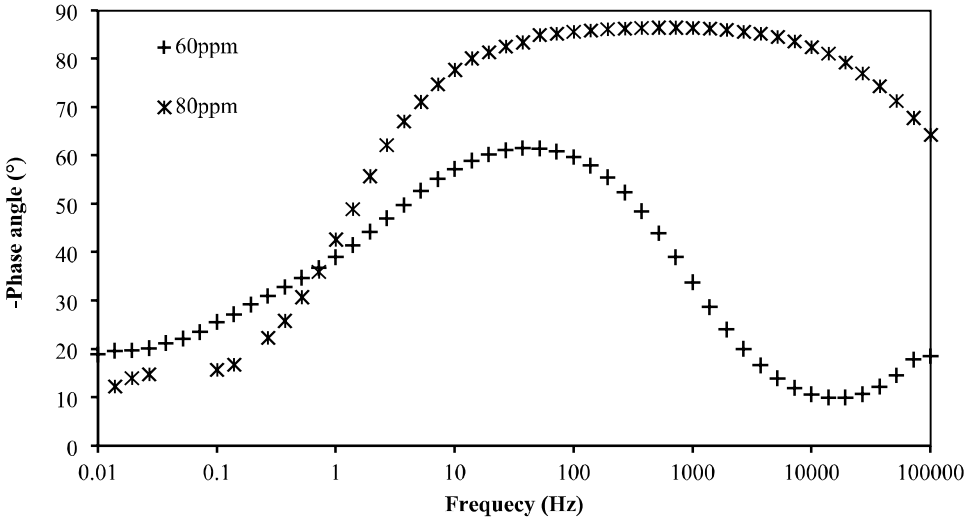

Fig. 14 Bode-phase plots of Cu–10Ni alloy specimen after 48 h of immersion in blank solution and solution containing 40 ppm MBT

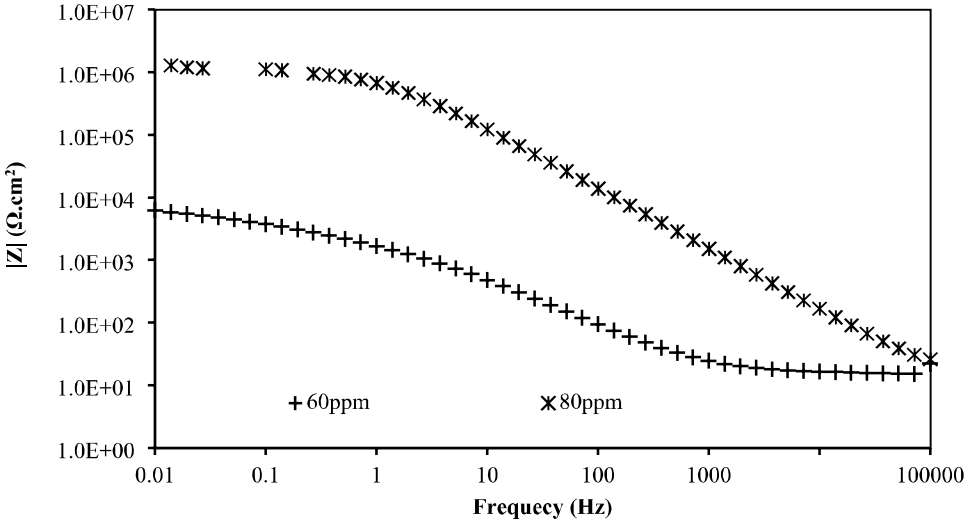

Fig. 15 Bode-modulus plots of Cu–10Ni alloy specimen after 48 h of immersion in blank solution and solution containing 40 ppm MBT

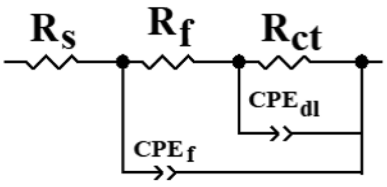

Fig. 16 EEC was used to fit the impedance results obtained for Cu–10Ni alloy specimen after 48 h of immersion in blank solution and solution containing 60 and 80 ppm MBT

MBT, the Ni content was about 12 wt%, implying a slight Ni enrichment. These observations confirm the inhibition effects of MBT above a specific concentration.

Nyquist, Bode-phase, and Bode-modulus plots of Cu–10Ni alloy obtained after 48 h of immersion in 3 wt% NaCl solution containing 60 ppm MBT (the inset) and 80 ppm MBT are shown in Fig. 13, 14, and 15. A new EEC model was proposed and used to fit the experimental data, as shown in Fig. 16. The value of the EEC parameters is presented in Table 4. It can be seen that the impedance value of the specimen increases with increasing the MBT concentration, especially at the concentration of 80 ppm. In the high-frequency region of the Bode diagrams, the impedance reaches a constant value independent of the frequency, and the phase angle tends towards 0°, which relates to the uncompensated or solution resistance (R_s). In the middle-frequency region, impedance and the frequency show a linear relationship, and the phase angle tends to − 60°. In the low-frequency region, impedance tends to become independent of frequency, but constant amplitude is not reached, attributed to the diffusion of the ionic species through the adsorbed inhibitor film. In Fig. 15, the phase maximum at the middle-frequency region broadens in the presence of 80 ppm of MBT, which implies the formation of a more protective layer of adsorbed inhibitors [40]. The phase angle at low frequencies does not approach 0°, implying the diffusion of ionic species through the adsorbed inhibitor film. The proposed EEC model involves two time-constants in series with the solution resistance (R_s). The first time-constant (R_fCPE_f) represents the properties of the adsorbed inhibitor film and the second time-constant in the low-frequency region represents the charge-transfer resistance and the constant phase element related to the double-layer capacitor at the metal surface. The adsorbed film thickness ($1/C_f$) increases with increasing the MBT concentration, and the film resistance (R_f) increases considerably in the solution containing 80 ppm MBT. This observation indicates the better protective ability of the film formed at the MBT concentration of 80 ppm. Comparing the R_{ct} values show that with increasing the MBT concentration, the R_{ct} value increases. It has been suggested that the inhibition mechanism of MBT for pure Cu depends on the nature of the binding between Cu(I) and the MBT and the properties of the copper oxide [36]. In the current work, the observed behavior can be attributed to the Ni enrichment of the oxide film formed on the surface and the role of the adsorbed film of inhibitor, which hinders the Ni leaching out from the oxide mentioned before. This enrichment increases R_{ct} value and leads to the higher corrosion resistance of the corrosion product film at the presence of 80 ppm MBT. The polarization resistance (R_p) value ($R_p = R_{ct} + R_f$) shows that the corrosion resistance increases with increasing the MBT concentration. Better inhibition performance obtained for specimens immersed in the solution containing 80 ppm MBT is attributed to the formation of a more compact and dense adsorbed inhibitor film. Decreasing the C_{pf} value with increasing the MBT concentration from 60 to 80 ppm confirms the formation of a thicker adsorbed inhibitor film.

Comparing the results obtained for different concentrations of MBT shows that EIS results are consistent with the results obtained from weight loss and polarization tests and show that there is a critical concentration for MBT to act as an effective inhibitor for Cu–10Ni alloys in 3 wt% NaCl solution.

4 Conclusion

The current study reports the effect of MBT on the corrosion inhibition of Cu–10Ni alloy in 3 wt% NaCl solution as a function of MBT concentration. Different methods, including Weight loss, potentiodynamic polarization, and EIS, were used. XPS and SEM were also used to characterize the surface of the specimen. All the methods' results were in good agreement and showed that the inhibition effect of MBT is a function of its concentration. Adding 40 ppm MBT to 3 wt% NaCl solution accelerates the corrosion rate of

Table 4 Parameters obtained from fitting the EIS data obtained for Cu–10Ni alloy specimen after 48 h of immersion in 3 wt% NaCl solutions containing 60 and 80 ppm MBT

Solution	R_s (Ω)	R_{ct} (kΩ cm^2)	CPE_{dl}		C_{dl} (μF cm^2)	CPE_{pf}		C_f (μF cm^{-2})	R_f (kΩ cm^2)	R_p (kΩ cm^2)	χ^2 ($\times 10^{-3}$)
			Q ($\times 10^{-5}$)	n		Q ($\times 10^{-5}$)	n				
60 ppm	10.2	10.909	31.51	0.36	1.4297	7.008	0.78	0.857	1.36	12.269	0.4
80 ppm	9.87	1362.6	0.2683	0.42	1.5452	0.057	0.95	0.264	807	2169.6	5.1

Cu–10Ni alloy and leads to localized attack. At the concentration of 60 and 80 ppm, MBT acts as an effective inhibitor, and the IE increases with increasing the MBT concentration. MBT adsorbed onto the surface through both N and S atoms of the inhibitor. The maximum IE of about 92% can be achieved at the concentration of 80 ppm. MBT adsorption into the surface can cease the Ni dealloying of the specimen and leads to better corrosion resistance.

Declarations

Conflict of interest The authors declare that they have no conflict of interest.

References

1. Chandra K, Mahanti A, Singh AP et al (2019) Microbiologically influenced corrosion of 70/30 cupronickel tubes of a heat-exchanger. Eng Fail Anal 105:1328–1339. https://doi.org/10.1016/j.engfailanal.2019.08.005
2. Dadić Z, Gudić S, Vrsalović L et al (2019) Different corrosion behaviour of CuNi10Fe1Mn alloy condenser tubes in seawater. Mech Technol Struct Mater 2019:25–31
3. Elragei O, Elshawesh F, Ezuber HM (2010) Corrosion failure 90/10 cupronickel tubes in a desalination plant. Desalin Water Treat 21:17–22. https://doi.org/10.5004/dwt.2010.1156
4. Ahmad Z, Aleem BJA (1994) The corrosion performance of 90–10 cupronickel in Arabian Gulf water containing ammonia. Desalination 95:307–323. https://doi.org/10.1016/0011-9164(94)00067-0
5. Chandra K, Kain V, Dey GK et al (2010) Failure analysis of cupronickel evaporator tubes of a chilling plant. Eng Fail Anal 17:587–593. https://doi.org/10.1016/j.engfailanal.2009.10.014
6. Agarwal DC (2002) Effect of ammoniacal sea water on material properties of copper-nickel alloy. Br Corros J 37:105–113. https://doi.org/10.1179/000705902225004329
7. Varea A, Pellicer E, Pané S et al (2012) Mechanical properties and corrosion behaviour of nanostructured Cu-rich CuNi electrodeposited films. Int J Electrochem Sci 7:1288–1302
8. Agarwal DC, Bapat AM (2009) Effect of ammonia and sulphide environment on 90/10 and 70/30 cupronickel alloy. J Fail Anal Prev 9:444–460. https://doi.org/10.1007/s11668-009-9281-7
9. Hopkinson BE (1964) Copper–nickel alloys for feed-water heater service. Corrosion 20:80t–88t. https://doi.org/10.5006/0010-9312-20.3.80t
10. Milošev I, Metikoš-Huković M (1997) The behaviour of Cu-xNi (x = 10 to 40 wt%) alloys in alkaline solutions containing chloride ions. Electrochim Acta 42:1537–1548. https://doi.org/10.1016/S0013-4686(96)00315-5
11. Kamkin AN, Davydov AD, Zhou G-D, Marichev VA (1999) Anodic oxide films on copper-nickel alloys. Russ J Electrochem 35:531–539
12. Sharma SB, Maurice V, Klein LH, Marcus P (2020) Local inhibition by 2-mercaptobenzothiazole of early stage intergranular corrosion of copper. J Electrochem Soc 167:161504. https://doi.org/10.1149/1945-7111/abcc36
13. Muñoz AI, Antón JG, Guiñón JL, Pérez Herranz V (2004) Comparison of inorganic inhibitors of copper, nickel and copper-nickels in aqueous lithium bromide solution. Electrochim Acta 50:957–966. https://doi.org/10.1016/j.electacta.2004.07.048
14. Gonçalves RS, Azambuja DS, Serpa Lucho AM (2002) Electrochemical studies of propargyl alcohol as corrosion inhibitor for nickel, copper, and copper/nickel (55/45) alloy. Corros Sci 44:467–479. https://doi.org/10.1016/S0010-938X(01)00069-5
15. Khadom AA, Yaro AS, Musa AY et al (2012) Corrosion inhibition of copper-nickel alloy: experimental and theoretical studies. J Korean Chem Soc 56:406–415. https://doi.org/10.5012/jkcs.2012.56.4.406
16. Hu X (2015) Study on inhibitors of copper and copper–nickel alloy in LiBr solution. Light Metals 2015:379–385. https://doi.org/10.1002/9781119093435.ch63
17. Hao C, Yin RH, Wan ZY et al (2008) Electrochemical and photoelectrochemical study of the self-assembled monolayer phytic acid on cupronickel B30. Corros Sci 50:3527–3533. https://doi.org/10.1016/j.corsci.2008.09.016
18. Kristan Mioč E, Hajdari Gretić Z, Otmačić Ćurković H (2018) Modification of cupronickel alloy surface with octadecylphosphonic acid self-assembled films for improved corrosion resistance. Corros Sci 134:189–198. https://doi.org/10.1016/j.corsci.2018.02.021
19. Appa Rao BV, Chaitanya Kumar K, Boyapati VAR, Kanukula CK (2013) Corrosion inhibition of Cu–Ni (90/10) alloy in seawater and sulphide-polluted seawater environments by 1,2,3-benzotriazole. ISRN Corros 2013:1–22. https://doi.org/10.1155/2013/703929
20. Obot IB, Meroufel A, Onyeachu IB et al (2019) Corrosion inhibitors for acid cleaning of desalination heat exchangers: progress, challenges and future perspectives. J Mol Liq 296:111760. https://doi.org/10.1016/j.molliq.2019.111760
21. Khadom AA, Yaro AS, Kadhum AAH (2010) Adsorption mechanism of benzotriazole for corrosion inhibition of copper-nickel alloy in hydrochloric acid. J Chil Chem Soc 55:150–152. https://doi.org/10.4067/S0717-97072010000100035
22. Jiang B, Jiang SL, Liu X et al (2015) Corrosion inhibition performance of triazole derivatives on copper–nickel alloy in 3.5 wt.% NaCl solution. J Mater Eng Perform 24:4797–4808. https://doi.org/10.1007/s11665-015-1759-8
23. Khadom AA (2014) Effect of temperature on corrosion inhibition of copper–nickel alloy by tetraethylenepentamine under flow conditions. J Chil Chem Soc 59:2545–2549. https://doi.org/10.4067/S0717-97072014000300004
24. Khadom AA, Yaro AS (2011) Modeling of corrosion inhibition of copper-nickel alloy in hydrochloric acid by benzotriazole. Russ J Phys Chem A 85:2005–2012. https://doi.org/10.1134/S0036024411110148
25. Khadom AA, Yaro AS, Kadum AAH (2010) Corrosion inhibition by naphthylamine and phenylenediamine for the corrosion of copper-nickel alloy in hydrochloric acid. J Taiwan Inst Chem Eng 41:122–125. https://doi.org/10.1016/j.jtice.2009.08.001
26. Maciel JM, Jaimes RFVV, Corio P et al (2008) The characterisation of the protective film formed by benzotriazole on the 90/10 copper-nickel alloy surface in H_2SO_4 media. Corros Sci 50:879–886. https://doi.org/10.1016/j.corsci.2007.10.011
27. Saifi H, Bernard MC, Joiret S et al (2010) Corrosion inhibitive action of cysteine on Cu-30Ni alloy in aerated 0.5 M H_2SO_4. Mater Chem Phys 120:661–669. https://doi.org/10.1016/j.matchemphys.2009.12.011
28. Martinez S, Metikoš-Huković M (2006) The inhibition of copper-nickel alloy corrosion under controlled hydrodynamic condition in seawater. J Appl Electrochem 36:1311–1315. https://doi.org/10.1007/s10800-005-9101-z
29. Omar IH, Zucchi F, Trabanelli G (1986) Schiff bases as corrosion inhibitors of copper and its alloys in acid media. Surf Coat Technol 29:141–151. https://doi.org/10.1016/0257-8972(86)90025-3
30. Trachli B, Keddam M, Takenouti H, Srhiri A (2002) Protective effect of electropolymerized 3-amino 1,2,4-triazole towards

corrosion of copper in 0.5 M NaCl. Corros Sci 44:997–1008. https://doi.org/10.1016/S0010-938X(01)00124-X
31. Otmačić H, Stupnišek-Lisac E (2003) Copper corrosion inhibitors in near neutral media. Electrochim Acta 48:985–991. https://doi.org/10.1016/S0013-4686(02)00811-3
32. El Issami S (2002) Inhibition de la corrosion du cuivre en milieu HCl 0,5 M par les composes organiques de type triazoleInhibition of copper corrosion in HCl 0.5 M medium by some triazolic compounds. Ann Chim Sci Matér 27:63–72. https://doi.org/10.1016/S0151-9107(02)80019-8
33. Hammouda N, Chadli H, Guillemot G, Belmokre K (2011) The corrosion protection behaviour of zinc rich epoxy paint in 3% NaCl solution. Adv Chem Eng Sci 01:51–60. https://doi.org/10.4236/aces.2011.12009
34. Huynh N, Bottle S, Notoya T et al (2002) Studies on alkyl esters of carboxybenzotriazole as inhibitors for copper corrosion. Corros Sci 44:1257–1276. https://doi.org/10.1016/S0010-938X(01)00109-3
35. Antonijevic MM, Petrovic MB, Petrović MB, Mihajlović MMA (2008) copper corrosion inhibitors: a review. Int J Electrochem Sci 3:1–28. https://doi.org/10.1016/j.ijengsci.2004.12.001
36. Sutter EMM, Ammeloot F, Pouet MJ et al (1999) Heterocyclic compounds used as corrosion inhibitors: correlation between 13C and 1H NMR spectroscopy and inhibition efficiency. Corros Sci 41:105–115. https://doi.org/10.1016/S0010-938X(98)00099-7
37. Benmessaoud M, Es-salah K, Hajjaji N et al (2007) Inhibiting effect of 2-mercaptobenzimidazole on the corrosion of Cu–30Ni alloy in aerated 3% NaCl in presence of ammonia. Corros Sci 49:3880–3888. https://doi.org/10.1016/j.corsci.2007.03.017
38. Allam NK, Ashour EA, Hegazy HS et al (2005) Effects of benzotriazole on the corrosion of Cu10Ni alloy in sulfide-polluted salt water. Corros Sci 47:2280–2292. https://doi.org/10.1016/j.corsci.2004.09.014
39. Babić R, Metikoš-Huković M, Lončar M (1999) Impedance and photoelectrochemical study of surface layers on Cu and Cu–10Ni in acetate solution containing benzotriazole. Electrochim Acta 44:2413–2421. https://doi.org/10.1016/S0013-4686(98)00367-3
40. Badawy WA, Ismail KM, Fathi AM (2006) Corrosion control of Cu–Ni alloys in neutral chloride solutions by amino acids. Electrochim Acta 51:4182–4189. https://doi.org/10.1016/j.electacta.2005.11.037
41. Badawy WA, Ismail KM, Fathi AM (2005) Environmentally safe corrosion inhibition of the Cu–Ni alloys in acidic sulfate solutions. J Appl Electrochem 35:879–888. https://doi.org/10.1007/s10800-005-4741-6
42. Kovačević N, Kokalj A (2013) The relation between adsorption bonding and corrosion inhibition of azole molecules on copper. Corros Sci 73:7–17. https://doi.org/10.1016/j.corsci.2013.03.016
43. Khiati Z, Othman A, Sanchez-Moreno M et al (2011) Corrosion inhibition of copper in neutral chloride media by a novel derivative of 1,2,4-triazole. Corros Sci 53:3092–3099. https://doi.org/10.1016/j.corsci.2011.05.042
44. Hu L, Zhang S, Li W, Hou B (2010) Electrochemical and thermodynamic investigation of diniconazole and triadimefon as corrosion inhibitors for copper in synthetic seawater. Corros Sci 52:2891–2896. https://doi.org/10.1016/j.corsci.2010.04.038
45. Otmacic Curkovic H, Stupnisek-Lisac E, Takenouti H (2009) Electrochemical quartz crystal microbalance and electrochemical impedance spectroscopy study of copper corrosion inhibition by imidazoles. Corros Sci 51:2342–2348. https://doi.org/10.1016/j.corsci.2009.06.018
46. Elbakri M, Touir R, EbnTouhami M et al (2008) Electrosynthesis of adherent poly(3-amino-1,2,4-triazole) films on brass prepared in nonaqueous solvents. Corros Sci 50:1538–1545. https://doi.org/10.1016/j.corsci.2008.02.014
47. Wu X, Wiame F, Maurice V, Marcus P (2020) Moiré structure of the 2-mercaptobenzothiazole corrosion inhibitor adsorbed on a (111)-oriented copper surface. J Phys Chem C 124:15995–16001. https://doi.org/10.1021/acs.jpcc.0c04083
48. Chen YH, Erbe A (2018) The multiple roles of an organic corrosion inhibitor on copper investigated by a combination of electrochemistry-coupled optical in situ spectroscopies. Corros Sci 145:232–238. https://doi.org/10.1016/j.corsci.2018.09.018
49. Faltermeier RB (1995) The evaluation of corrosion inhibitors for application to copper and copper alloy archaeological artefacts by, 1–332
50. Zhang H, Xiong S (2018) A review on experimental studies of corrosion inhibitor adsorption on copper surface. IOP Conf Ser Mater Sci Eng. https://doi.org/10.1088/1757-899X/439/4/042001
51. Naumkin AV, Kraut-Vass A, Gaarenstroom SW (2003) NIST standard reference database 20, version 4.1
52. Finšgar M, Fassbender S, Nicolini F, Milošev I (2009) Polyethyleneimine as a corrosion inhibitor for ASTM 420 stainless steel in near-neutral saline media. Corros Sci 51:525–533. https://doi.org/10.1016/j.corsci.2008.12.006
53. Kartsonakis IA, Stamatogianni P, Karaxi EK, Charitidis CA (2019) Comparative study on the corrosion inhibitive effect of 2-mecraptobenzothiazole and Na_2HPO_4 on industrial conveying Api 5l x42 pipeline steel. Appl Sci 10:290. https://doi.org/10.3390/app10010290
54. Zhang Z, Wang Q, Wang X, Gao L (2017) The influence of crystal faces on corrosion behavior of copper surface: first-principle and experiment study. Appl Surf Sci 396:746–753. https://doi.org/10.1016/j.apsusc.2016.11.020
55. Vernack E, Costa D, Tingaut P, Marcus P (2020) DFT studies of 2-mercaptobenzothiazole and 2-mercaptobenzimidazole as corrosion inhibitors for copper. Corros Sci 174:108840. https://doi.org/10.1016/j.corsci.2020.108840
56. Sherif EM, Park S-M (2005) Inhibition of Copper Corrosion in 3.0% NaCl Solution by N-Phenyl-1,4-phenylenediamine. J Electrochem Soc 152:428. https://doi.org/10.1149/1.2018254
57. Badawy WA, Ismail KM, Fathi AM (2005) Effect of Ni content on the corrosion behavior of Cu–Ni alloys in neutral chloride solutions. Electrochim Acta 50:3603–3608. https://doi.org/10.1016/j.electacta.2004.12.030
58. Dhar HP, White RE, Burnell G et al (1985) Corrosion of Cu and Cu–Ni alloys in 0. 5M NaCl and in synthetic seawater. Corrosion 41:317–323. https://doi.org/10.5006/1.3582011
59. Blundy RG, Pryor MJ (1972) The potential dependence of reaction product composition on copper-nickel alloys. Corros Sci 12:65–75. https://doi.org/10.1016/S0010-938X(72)90567-7
60. Khaled KF (2011) Studies of the corrosion inhibition of copper in sodium chloride solutions using chemical and electrochemical measurements. Mater Chem Phys 125:427–433. https://doi.org/10.1016/j.matchemphys.2010.10.037
61. Kabasakaloğlu M, Kıyak T, Şendil O, Asan A (2002) Electrochemical behavior of brass in 0.1 M NaCl. Appl Surf Sci 193:167–174. https://doi.org/10.1016/S0169-4332(02)00258-1
62. Finšgar M, Kek Merl D (2014) An electrochemical, long-term immersion, and XPS study of 2-mercaptobenzothiazole as a copper corrosion inhibitor in chloride solution. Corros Sci 83:164–175. https://doi.org/10.1016/j.corsci.2014.02.016
63. Levi M (2001) Application of finite-diffusion models for the interpretation of chronoamperometric and electrochemical impedance responses of thin lithium insertion V_2O_5 electrodes. Solid State Ionics 143:309–318. https://doi.org/10.1016/S0167-2738(01)00819-0
64. Kim C-H, Pyun S-I, Kim J-H (2003) An investigation of the capacitance dispersion on the fractal carbon electrode with edge and basal orientations. Electrochim Acta 48:3455–3463. https://doi.org/10.1016/S0013-4686(03)00464-X

65. Jorcin J-B, Orazem ME, Pébère N, Tribollet B (2006) CPE analysis by local electrochemical impedance spectroscopy. Electrochim Acta 51:1473–1479. https://doi.org/10.1016/j.electacta.2005.02.128
66. Lukács Z (1999) Evaluation of model and dispersion parameters and their effects on the formation of constant-phase elements in equivalent circuits. J Electroanal Chem 464:68–75. https://doi.org/10.1016/S0022-0728(98)00471-9
67. Kek-Merl D, Lappalainen J, Tuller HL (2006) Electrical properties of nanocrystalline CeO[sub 2] thin films deposited by in situ pulsed laser deposition. J Electrochem Soc 153:J15. https://doi.org/10.1149/1.2165778
68. Barsoukov E, Macdonald JR (2005) Impedance spectroscopy. Wiley, Hoboken
69. Finšgar M, Merl DK (2014) 2-Mercaptobenzoxazole as a copper corrosion inhibitor in chloride solution: Electrochemistry, 3D-profilometry, and XPS surface analysis. Corros Sci 80:82–95. https://doi.org/10.1016/j.corsci.2013.11.022

Authors and Affiliations

Arman Zarebidaki[1] · Seyed Haman Hedaiat Mofidi[1] · Farzaneh Iranmanesh Bahri[1]

✉ Arman Zarebidaki
a.zarebidaki@aut.ac.ir

[1] Corrosion Engineering and Material Protection Group, Bandar Abbas Campus, Amirkabir University of Technology (Tehran Polytechnic), P.O. Box 15875-4413, Tehran, Iran